Title

Visualizing red blood cell sickling and the effects of inhibition of sphingosine kinase 1 using soft X-ray tomography

Journal

Journal of Cell Science, 129(18)

ISSN

0021-9533

Authors

Darrow, Michele C
Zhang, Yujin
Cinquin, Bertrand P
et al.

Publication Date

2016-09-15

DOI

10.1242/jcs.189225

Peer reviewed

© 2016. Published by The Company of Biologists Ltd | Journal of Cell Science (2016) 129, 3511-3517 doi:10.1242/jcs.189225

TOOLS AND TECHNIQUES

Visualizing red blood cell sickling and the effects of inhibition of sphingosine kinase 1 using soft X-ray tomography

Michele C. Darrow[1,*], Yujin Zhang[2], Bertrand P. Cinquin[3,4,‡], Elizabeth A. Smith[3,4], Rosanne Boudreau[3,4], Ryan H. Rochat[1,§], Michael F. Schmid[1], Yang Xia[2,5,6], Carolyn A. Larabell[3,4,¶] and Wah Chiu[1,¶]

ABSTRACT

Sickle cell disease is a destructive genetic disorder characterized by the formation of fibrils of deoxygenated hemoglobin, leading to the red blood cell (RBC) morphology changes that underlie the clinical manifestations of this disease. Using cryogenic soft X-ray tomography (SXT), we characterized the morphology of sickled RBCs in terms of volume and the number of protrusions per cell. We were able to identify statistically a relationship between the number of protrusions and the volume of the cell, which is known to correlate to the severity of sickling. This structural polymorphism allows for the classification of the stages of the sickling process. Recent studies have shown that elevated sphingosine kinase 1 (Sphk1)-mediated sphingosine 1-phosphate production contributes to sickling. Here, we further demonstrate that compound 5C, an inhibitor of Sphk1, has anti-sickling properties. Additionally, the variation in cellular morphology upon treatment suggests that this drug acts to delay the sickling process. SXT is an effective tool that can be used to identify the morphology of the sickling process and assess the effectiveness of potential therapeutics.

KEY WORDS: Cryogenic soft X-ray tomography, Red blood cell, Sickle cell disease, Sphingosine kinase inhibitor, Red cell morphology

INTRODUCTION

Sickle cell disease (SCD) was first identified in 1910 by James Herrick (Herrick, 1910). In 1949, SCD was the first disease that was understood on the molecular level, when Linus Pauling suggested that the sickling of a red blood cell (RBC) was caused by a structural difference in the hemoglobin present in RBCs (Pauling et al., 1949). In 1957, this structural difference was explained genetically by Vernon Ingram as a single amino acid substitution in sickle hemoglobin (Ingram, 1957). In 2008, it was estimated that globally, ∼287,500 children are born with SCD (Rees et al., 2010). The prevalence of SCD in the USA is ∼1 in 4000 people (Hassell, 2010) and is much higher in other geographical regions. Even though we have known about this disease for over a century, there is still an acute lack of effective preventative approaches or mechanism-specific treatment options (Rees et al., 2010). Hydroxyurea is currently the only approved treatment for SCD (Rees et al., 2010). Although the actual mechanism of action is unknown, it is generally accepted that hydroxyurea increases the level of fetal hemoglobin (HbF), reducing the rate of sickle hemoglobin (HbS) fibril formation (Akinsheye et al., 2011; Noguchi et al., 1988).

The structure and function of hemoglobin were elucidated by Max Perutz (Perutz et al., 1960) and has since been understood in more detail with improved structural resolution (Harrington et al., 1997; Padlan and Love, 1985). SCD is an autosomal recessive genetic disease caused by a single point mutation in the β-globin subunit of hemoglobin that changes the negatively charged glutamic acid residue to a hydrophobic valine residue, resulting in non-covalent polymerization and double-strand formation under low-oxygen conditions. Polymerization occurs through hydrophobic lateral contacts involving the mutant valine residues of one HbS molecule and axial contacts in the β-globin subunit of an adjacently located HbS molecule (Rodgers et al., 1987). Studies of HbS fibers by negative stain electron microscopy have demonstrated that hemoglobin bundles are composed of at least seven double strands (Carragher et al., 1988; Dykes et al., 1978, 1979). Formation and elongation of these bundles occurs through a double nucleation mechanism and leads to RBC distortion. Upon reoxygenation, the hemoglobin fibers rapidly dissolve allowing the RBCs to assume their normal shapes. Repeated sickling episodes causes damage to the cell membrane, which decreases the elasticity of the cell and its ability to return to a normal biconcave disc shape when normoxyic conditions are restored. There are many factors that can influence the process of sickling, including oxygen saturation, pH, temperature and HbF levels (Christoph et al., 2005; Noguchi and Schechter, 1981).

The loss of membrane elasticity plays a key role in the pathophysiology of the disease. RBCs must be highly elastic in order to pass through the smaller capillary blood vessels to deliver oxygen to tissue. Cells that have undergone multiple episodes of sickling are more rigid and become trapped in the narrow capillaries, leading to vascular occlusion and ischemia (Rees et al., 2010; Sorette et al., 1987). Additionally, rigid cells that are unable to return to their normal shape are identified and destroyed in a process called hemolysis (Frenette and Atweh, 2007; Presley et al., 2010; Rees et al., 2010). Although new RBCs are continuously created, this happens at a lower rate and cannot compensate for all of the destroyed cells, leading to anemia.

[1]National Center for Macromolecular Imaging, Verna and Marrs McLean Department of Biochemistry and Molecular Biology, Baylor College of Medicine, Houston, TX 77030, USA. [2]Department of Biochemistry and Molecular Biology, University of Texas Health Science Center at Houston, Houston, TX 77030, USA. [3]Department of Anatomy, University of California San Francisco, San Francisco, CA 94143, USA. [4]Physical Biosciences Division, Lawrence Berkeley National Laboratory, Berkeley, CA 94720, USA. [5]University of Texas at Houston Graduate School of Biomedical Sciences, Houston, TX 77030, USA. [6]Department of Nephrology, The First Xiangya Hospital, Central South University, Changsha, Hunan 410008, People's Republic of China.
*Present address: Life Science Division, B24, Diamond Light Source Ltd, Harwell Campus, Oxfordshire, OX11 0DE, UK. ‡Present address: École Normale Supérieure de Cachan, 61 Avenue du Président Wilson, Cachan 94230, France. §Present address: Baylor College of Medicine Residency Program – Pediatrics, Texas Children's Hospital, Houston, TX 77030, USA.

¶Author for correspondence (wah@bcm.edu; carolyn.larabell@ucsf.edu)

W.C., 0000-0002-8910-3078

Received 11 March 2016; Accepted 1 August 2016

Journal of Cell Science (2016) 129, 3511-3517 doi:10.1242/jcs.189225

Clinically, hallmarks of SCD include changes to RBC morphology, and RBC density increase (volume decrease) under low-oxygen conditions. In both cases, the extent of the changes are associated with the clinical symptomatology, suggesting that both density and morphology changes might be determinants of disease severity (Brittenham et al., 1985; Brugnara, 2003; Charache and Conley, 1964; Kumar et al., 2014). The morphology of sickled RBCs has been studied extensively using light microscopy (Christoph et al., 2005; Coletta et al., 1988; Horiuchi et al., 1988; Pierre, 2002; van Beers et al., 2014; Zhang et al., 2014) and scanning electron microscopy (SEM; Horiuchi et al., 1988; Kaul and Xue, 1991; Pierre, 2002) to gather information on cell morphology. In fact, preclinical trials and treatment-testing experiments routinely use light-microscopy-derived percentages of sickled cells as predictors of outcome (Abdulmalik et al., 2005; Chang et al., 1983a,b; Ikuta et al., 2011; Zhang et al., 2014). However, both light microscopy and SEM provide only two-dimensional data and, in the case of light microscopy, at relatively low resolution. To address these shortcomings, here we have used soft X-ray tomography (SXT) to three-dimensionally characterize RBC morphology throughout the sickling process, providing new structural insights into the sizes and shapes of sickled RBCs. Additionally, we have used this new methodology to structurally characterize the morphological effects of the anti-sickling drug compound 5C.

RESULTS

SXT of sickled RBCs

SXT at cryo-temperatures bridges the gap between light and electron microscopy, allowing the imaging of whole cells without sectioning techniques at a resolution greater than light microscopy (~50 nm). SXT uses the inherent contrast of fully hydrated specimens by imaging in the 'water window' (2.4 nm wavelength, 517 eV) where common biological elements such as carbon and nitrogen absorb X-rays and are therefore visible, whereas water is relatively transparent (Carzaniga et al., 2014; Larabell and Nugent, 2010; Le Gros et al., 2005; Patwardhan et al., 2014). Additionally, owing to the use of a thin-walled glass capillary tube to flash freeze and image the specimen, there is no visible radiation damage at the achievable resolution, and it is possible to collect projection image tilt series of 180° or greater allowing for a three-dimensional reconstruction with no distortions due to missing wedge artifacts as in electron microscopy (Larabell and Nugent, 2010; Le Gros et al., 2005, 2014; Parkinson et al., 2008). Variations of this technique have been successfully applied towards the understanding of changes in cellular morphology due to disease and/or treatment (Chichón et al., 2012; Hanssen et al., 2012; Myllys et al., 2016; Pérez-Berná et al., 2016).

Mature RBCs from mice expressing the human sequence of the β-subunit of hemoglobin, both SCD mutant and wild type (WT), were exposed to either low oxygen (hypoxia) or normal oxygen (normoxia) conditions for 2 hours. All samples were then lightly fixed using glutaraldehyde and then imaged.

In all, we imaged and reconstructed over 600 cells using SXT. Each of these cells was staged based on three-dimensional visual inspection of the number of protrusions. A total of 105 subtomograms of hypoxia-induced sickle cells from both the untreated and compound-5C-treated conditions were extracted and analyzed volumetrically. We did not find a statistical difference in volume between the untreated and compound-5C-treated groups (Fig. S1), so they were combined for overall volumetric analysis. The extracted sickle RBCs were classified by the number of protrusions (Fig. 1A). A protrusion is defined as an extended appendage, where the normal biconcave disc shape of a RBC has been deformed due to changes in the internal structures of the cell. Examples of protrusions can be seen in Fig. 1 and Fig. S2. The majority of sickle RBCs had four protrusions, but there were a few with more than 15 protrusions. Given that protrusions were found to extend in all directions three-dimensional analysis of cellular morphology was necessary for accurate protrusion counting (Fig. S2).

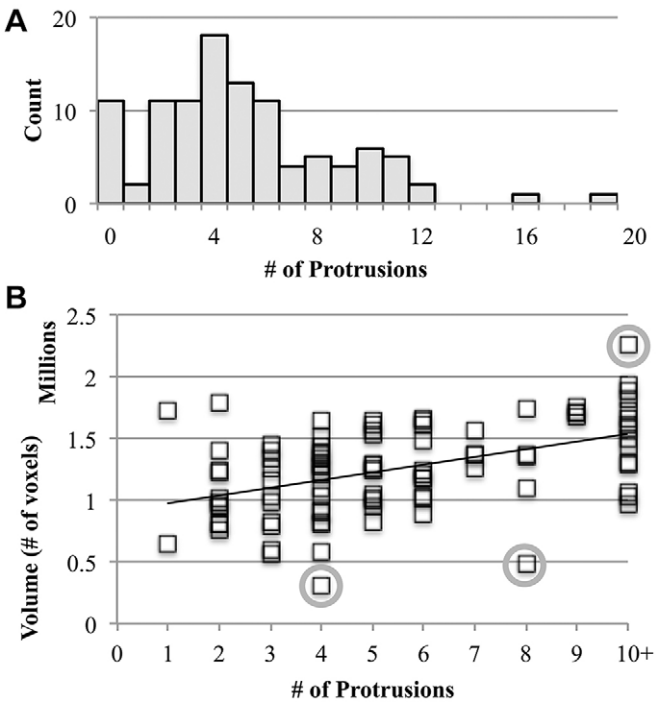

Fig. 1. The number of cell protrusions is correlated with volume, and therefore density. (A) Results from sickle RBCs under hypoxia conditions both with and without treatment with compound 5C were combined after statistical tests revealed no significant difference between the two populations (see also Fig. S1). This combined dataset (n=105) represents four individual SXT experiments. The distribution of cells based on number of protrusions for the combined dataset is shown. In subsequent presentations all RBCs with ≥10 protrusions were combined into a 10+ category. (B) Volumetric analysis of the combined sickle RBC dataset revealed a correlation between volume and the number of protrusions (see also Fig. S2). The volume measurement can be used as an inverse proxy for density, indicating the number of protrusions is correlated to density, a hallmark of SCD associated with severity of sickling. Circled data points have been statistically identified as outliers (as described in the Materials and Methods), but not excluded.

Volumetric and feature analysis of sickled RBCs

Dehydration of RBCs, and therefore higher cellular density, is a hallmark of SCD (Brugnara, 2003; Fabry et al., 1984; Kumar et al., 2014). When density is high, volume will be low, assuming a constant mass. Using these relationships, the 3D volume measurements from the subtomograms of individual RBCs can be used to describe the severity of cell sickling. Our measurements clearly show that lower volume (high density) correlates to lower protrusion numbers, whereas higher volume (low density) correlates to higher protrusion numbers (Fig. 1B). Using a linear regression test, this correlation is highly significant (P<0.01). Sickle RBCs with zero protrusions were not included in this statistical analysis because they are expected to, and do, have volumes that are similar to sickle RBCs in the 10+ protrusions group. Outliers were calculated on binned data using the interquartile range (IQR)

Journal of Cell Science (2016) 129, 3511-3517 doi:10.1242/jcs.189225

method, as described in the Materials and Methods, and are marked with gray circles, but not removed from analysis. Importantly, this statistical correlation is present regardless of treatment (Fig. S1).

Classification of sickle RBCs based on features

Based on the relationship between the number of protrusions and volume, the data were binned into four categories describing the severity of sickling on a per cell basis (Fig. 2). Because the progression of pathological severity of sickled RBCs is related to the reduction in volume, and a correlation exists between volume and protrusion numbers, the protrusion numbers can be used to indicate the severity of sickling or, when considered at a population level, the progression of the disease. To place our morphological observations into the context of RBC sickling, we describe them in four categories. The 'none' category contains cells with zero or one protrusion; the 'mild' category contains cells with eight, nine, ten or more protrusions (because of the small number of cells with more than ten protrusions, these were condensed into a single 10+ category); the 'moderate' category contains cells with five, six or seven protrusions; and lastly, the 'severe' category contains cells with two, three or four protrusions. It is worth noting that RBCs with one protrusion are likely due to crowding in the capillary tube, as one would not expect the hemoglobin fibrils to exert enough force to deform the membrane without having additional contacts with other areas of the membrane. For this reason, RBCs with one protrusion were included in the none category.

Using the categories defined above, RBCs from various control groups (WT cells, normoxia; WT cells, hypoxia; SCD cells, normoxia) and the experimental group (SCD cells, hypoxia) were classified based on protrusion number (Fig. 3). As expected, the vast majority of all three control populations were staged to the none category. The few RBCs (n=10; ∼4%) in the control groups that were staged to other categories potentially represent experimental error or false positives. The experimental group of SCD cells under hypoxia conditions differed significantly from these controls. Only 19±8% (mean±s.e.m.) of the population fell into the none category, with the rest split between the other three categories. The majority of this remainder (43±6%) fell into the severe category.

Effects of Sphk1 inhibitor on sickling process

We next used this classification system to determine the morphological effects of a potential drug treatment. Previous work has demonstrated that sphingosine kinase 1 (Sphk1) inhibitors significantly decreased sickling RBCs in mice (Zhang et al., 2014) and compound 5C has been shown to specifically inhibit Sphk1 (Datta et al., 2014; Tan et al., 2014; Wong et al., 2009). When comparing the staged sickle RBCs under hypoxia conditions, without and with treatment (Fig. 4), there was a statistically significant shift in the population of treated cells. Further statistical analysis using Tukey's multiple comparison test indicated that the shift in protrusion numbers due to treatment is towards the less severe categories of sickling. This result is affirmed by a significant pairwise χ^2 test between the moderate and severe categories, demonstrating the largest shift is from the severe to the moderate category in the compound-5C-treated population.

Upon assessment with light microscopy, ∼60% of sickle RBCs under hypoxia conditions and without compound 5C treatment, were categorized as sickled, whereas in the compound-5C-treated condition, there was a significant decrease in the proportion of sickled cells to ∼25% (Fig. 5). Beneficial effects of treatment with compound 5C were also observed in multiple biochemical assays, including erythrocyte survival times, where we found that compound 5C treatment significantly increased RBC lifespan (Fig. 6). Taken together, these results indicate that inhibition of Sphk1 activity can attenuate the severity of sickle RBC morphology changes.

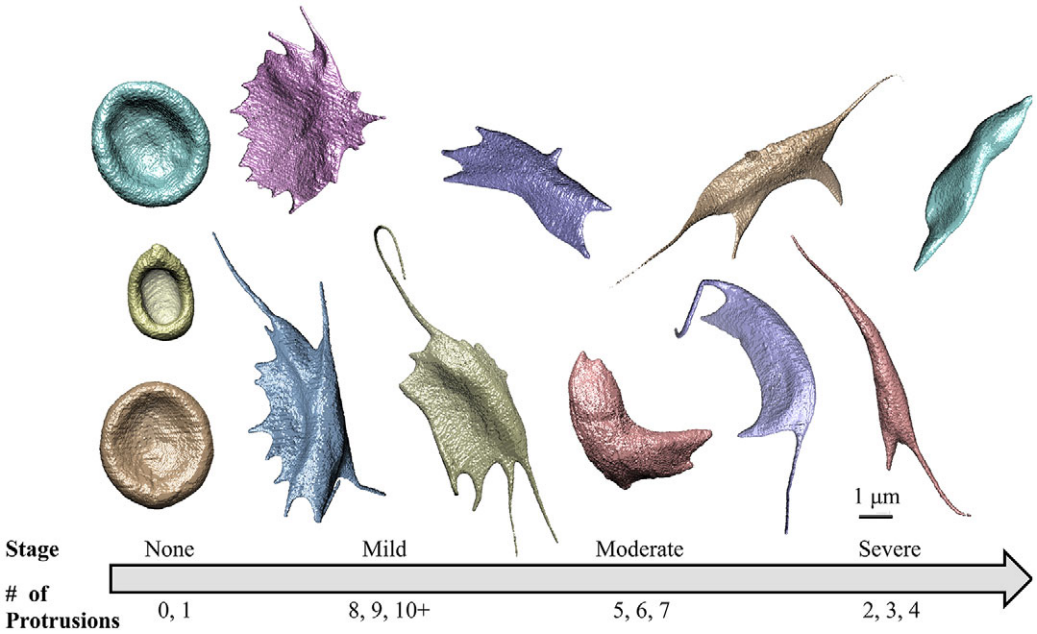

Fig. 2. Continuum of the stages of sickling. Following volumetric analysis to correlate protrusion number with density, a hallmark of SCD, data were binned into four categories. The none category is composed of RBCs with zero or one protrusion; the mild category is composed of RBCs with eight, nine, ten or greater protrusions; the moderate category is composed of RBCs with five, six or seven protrusions; and finally, the severe category is composed of RBCs with two, three or four protrusions. Multiple examples of RBCs as imaged by SXT that fall into each of these categories are displayed here (see also Fig. S2).

Journal of Cell Science (2016) 129, 3511-3517 doi:10.1242/jcs.189225

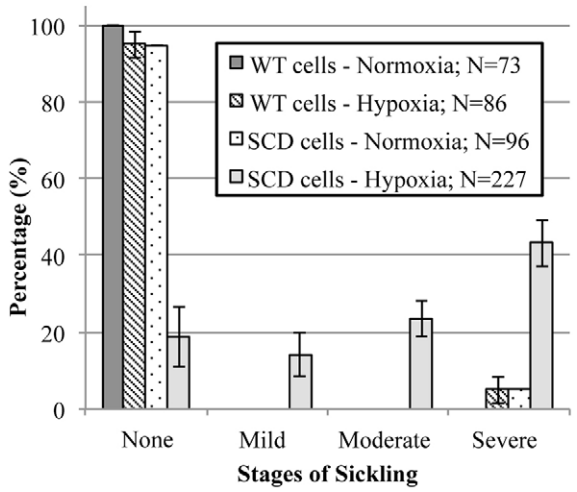

Fig. 3. Sickle RBCs under hypoxia conditions differ significantly from controls. Only 19±8% of cells from the experimental condition (SCD cells, hypoxia) fall into the none category. The rest of these cells was split unevenly throughout the remaining categories, with the majority falling into the severe category (43±6%), with 24±5% in the moderate category and 14±6% in the mild category. Importantly, these data indicate that up to 80% of the RBCs cultivated under these conditions (4% oxygen, 37°C, 2 h) are sickled to some degree. Note: data are presented as normalized mean±s.e.m. and represent four individual experiments.

DISCUSSION

The use of SXT in this study has provided the three-dimensional resolution necessary to unambiguously classify RBCs beyond the binary categories of 'biconcave disc' and 'aberrant' that are commonly used to describe sickle RBCs in light microscopy.

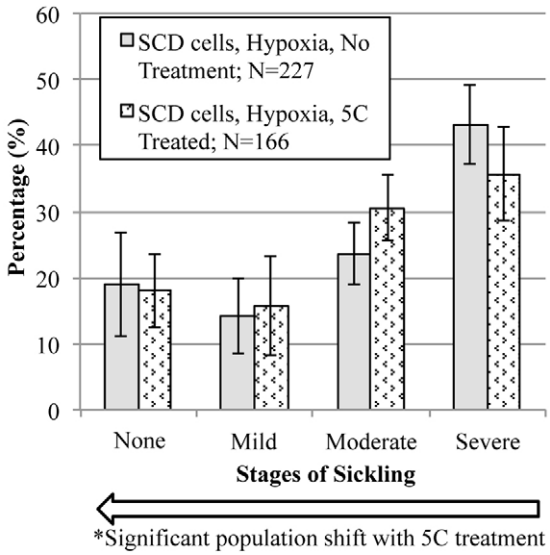

Fig. 4. Compound 5C significantly shifts the population of RBCs toward the less severe categories of sickling. One-way analysis of variance indicates that the population shift due to treatment with compound 5C is significant as compared to the control sickle RBC population (*P<0.05; see also Table S1). Tukey's multiple comparison test indicates that this shift is towards the less severe categories of sickling and a pairwise χ^2 test indicates the greatest change is between the moderate and severe categories. Taken together, these data indicate the treatment is acting to keep sickle RBCs in the morphological mild and moderate categories. Note: data are presented as normalized mean±s.e.m. and represent four individual experiments.

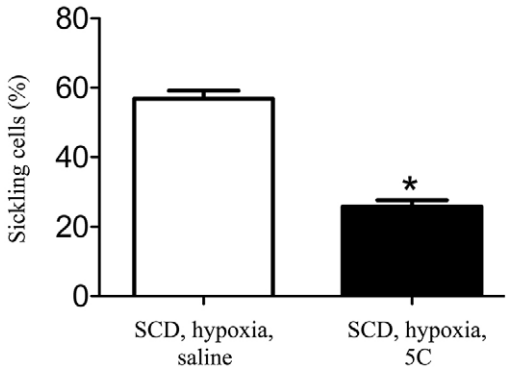

Fig. 5. Effects of compound 5C treatment on sickling RBCs using light microscopy. Inhibition of Sphk1 reduced sickling of SCD RBCs under hypoxia conditions. The percentage of sickled cells was significantly reduced in the RBCs treated with the Sphk1-specific inhibitor compound 5C. *P<0.05 versus saline treatment control (Student's t-test). Data are presented as mean±s.d. (n=1000).

Here, when comparing the two methodologies, ~20% of cells with sickling morphology were missed using light microscopy. Additionally, with three-dimensional data, we were able to fully characterize the intermediate state variously referred to as a 'holly leaf', 'wreath' or 'star' shape (Horiuchi et al., 1988; Kaul and Xue, 1991; Kumar et al., 2014). However, the total number of RBCs in the SXT analysis is smaller and the technique is more time intensive and, pending the production of lab-based X-ray microscopes, less available as compared to light microscopy. Using volume as an inverse proxy for density, we demonstrate that cell projection numbers and density are correlated, allowing for the staging of cells into four categories along the continuum of severity of sickling: none, mild, moderate and severe.

In vitro growth of microtubules in vesicles can be used as a model of membrane deformation due to fibril growth. In this model, deformation of the vesicle membrane occurs simultaneously at opposing points in the membrane and can lead to very long protrusions and an overall horseshoe, or sickled shape (Fygenson et al., 1997). The correlation between sickled RBCs with high protrusion numbers and high volumes implies there are many nucleation points for sickle fibril growth in these cells; by contrast, low sickle RBC volume and cells with a low protrusion number have undergone fibril growth for some time, causing the membrane to stretch and the fibrils to collapse down to only a few, in some cases highly elongated, protrusions. Tearing of the membrane due to

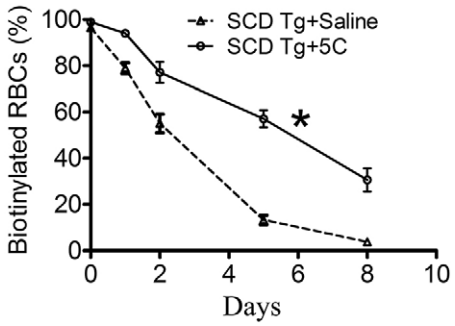

Fig. 6. Treatment of SCD mice by compound 5C increased the lifespan of RBCs. Specific inhibition of Sphk1 with 5C in SCD mice significantly increased RBC lifespan. *P<0.05 versus saline treatment control (Student's t-test). Data are presented as mean±s.e.m. (n=6).

Journal of Cell Science (2016) 129, 3511-3517 doi:10.1242/jcs.189225

fibril growth was only observed in two cases, both of which would be classified into the severe category. It is possible that the difference between the RBCs with a low protrusion number and high protrusion number is purely the number of cycles of deoxygenation and reoxygenation they have undergone, potentially damaging the membrane during each cycle, or not fully breaking down the fibrils between cycles. Unfortunately, this study is unable to distinguish between these possibilities.

Volumetric analysis of three-dimensional data requires successful reconstruction of tilt series and, when the cell is larger than the field of view of a single tilt series, merging of reconstructed datasets, followed by manual assignment of density. This is a time-consuming workflow that requires manual oversight and input at multiple steps. However, using the relationship between volume and protrusion number simplifies this process. Protrusion numbers can be identified using the original tilt series data, even before reconstruction. Because of this, a larger number of cells can be included in the protrusion number dataset than were included in the volumetric analysis. Using these stages to correlate protrusion numbers to severity of sickling, SXT is a novel and efficient method for collecting structural information about close-to-native state sickle RBCs.

The stages of sickling identified by the volumetric analysis allow us to characterize the percentage of cells at each stage both without and with a treatment. It is important to clarify that the category titles refer to the severity of sickling on a per cell basis, whereas the clinical progression of the disease would require assessment at the population level. The effects of compound 5C treatment are subtle, not changing the overall percentage of RBCs that are sickled (~80% with or without treatment) but instead shifting the population into different categories. The largest shift in the treated population is seen as a decrease in sickle RBCs in the severe category and an increase in sickle RBCs in the moderate and mild categories. The shift is not due to an increase in volume in the compound-5C-treated group, as statistical analysis showed no difference in volume by treatment (Fig. S1). These subtle changes in morphology would likely be missed using light microscopy or SEM due to the lower resolution of light microscopy and/or the two-dimensional nature of both of these imaging modalities. Indeed, as assessed by light microscopy, sickling morphology in compound-5C-treated cells is significantly decreased in treated compared to non-treated cells (Fig. 5), suggesting light microscopy is less effective at identification of the mild category or early stage sickling events, instead considering them non-sickled.

Sphingosine 1-phosphate (S1P) acts as a signaling molecule to regulate multiple distinct biological processes through interaction with cell surface S1P receptors and/or interactions with regulatory proteins (Spiegel and Milstien, 2003). For example, S1P has been shown to regulate progenitor cell egress from bone marrow (Ratajczak et al., 2010), lymphocyte egress from the thymus, spleen and lymph nodes (Pappu et al., 2007), to activate NF-κB, an inflammation control transcription factor (Alvarez et al., 2010), and to promote cell proliferation and angiogenesis (English et al., 2002). RBCs are the largest cellular reserve of S1P, partly due to the lack of enzymes that degrade S1P (Hänel et al., 2007; Ito et al., 2007). Recent research has shown that elevated Sphk1-mediated production of S1P contributes to sickling and disease progression (Zhang et al., 2014), indicating that S1P is acting intracellularly, independently of its receptors (Zhang et al., 2014). This makes Sphk1 an attractive target for mediation of S1P levels and therefore of SCD phenotypes. Here, we show the compound 5C is an effective potential modulator of sickled RBC morphology. Additionally, we show that the effect of inhibition of S1P accumulation is not volume related, but instead related to the slowing of the sickling process. This suggests that S1P interacts with hemoglobin, directly or indirectly, to stabilize the sickle hemoglobin fibrils, and when inhibited, leads to less fibril polymerization.

MATERIALS AND METHODS

Mice, treatment conditions and specimen collection

SCD Berkeley transgenic (Tg) mice, exclusively expressing human sickle hemoglobin (HbS), were purchased from The Jackson Laboratory, Inc. The SCD Tg mice were produced by breeding homozygous male with heterozygous female mice. Newborn mice were genotyped by PCR. Animal care was in accordance with institutional and NIH guidelines. Research protocols were reviewed and approved by the University of Texas Health Science Center at Houston Animal Welfare Committee.

SCD Tg mice, at 8 weeks of age, were divided into two groups. Mice were anesthetized by inhaling isoflurane. Osmotic minipumps (Alza) were implanted subcutaneously in the nape of the neck. Compound 5C was delivered at a rate of 2 mg/kg body weight per day for 28 days. Control mice received saline. 0.6–1 ml of the blood was withdrawn from anesthetized mouse heart. The blood was anticoagulated with heparin. Heparin-treated blood was used for *in vitro* treatment.

In vitro compound 5C treatment and hypoxia-induced sickling

Heparin-treated blood was centrifuged at 2400 ***g*** for 5 min at room temperature, followed by aspiration of the interface between the plasma and white blood cells. Cells were washed three times and resuspended in culture medium (F-10 Hams with 1% penicillin-streptomycin) to 4% hematocrit (HCT) and 1 ml of cells was placed into each well of a 12-well plate. The cells were treated with compound 5C (2 µg/ml, graciously provided by colleagues at the National University of Singapore) or saline and exposed to 4% oxygen, 96% nitrogen for 2 hours with shaking at 37°C. After treatment, the cells were fixed by placing in 0.3% glutaraldehyde in PBS that had 4% oxygen bubbled through. The fixed cells were used for light microscopy or SXT study. Prior to treatment, basic hematological parameters of blood from mice treated with saline and compound 5C were taken (Table S1).

Soft X-ray tomography

Samples were concentrated, transferred to thin-walled glass capillaries and plunge frozen in liquid propane (Le Gros et al., 2005). Imaging was performed at the National Center for X-ray Tomography at the Advanced Light Source of Lawrence Berkeley National Laboratory (LBNL) on the XM-2 soft X-ray microscope, which is equipped with a Fresnel zone-plate-based condenser and objective lenses (made by the Center for X-ray Optics, LBNL; Le Gros et al., 2014). The specimens were kept in an atmosphere of liquid nitrogen cooled helium gas at all times during imaging. For each dataset, two-dimensional projection images were collected in 2° steps through a total rotational range of greater than 180°. Exposure times between 150 and 300 ms were used (depending on synchrotron ring current). If changes due to radiation damage were seen during the tilt series or the presence of non-vitreous ice was detected, the data was excluded from assessment. During data collection, the microscope was equipped with a resolution-defining 50-nm objective lens. Reconstruction of tilt series into three-dimensional volumes was completed with the IMOD package (Kremer et al., 1996) based on manual alignment of images using fiducial markers. IMOD was also used for visual inspection to assess protrusion numbers. Avizo (http://fei.com) was used for manual segmentation and the measurement of voxel counts giving rise to the volume measurement for each cell, Amira (Pruggnaller et al., 2008) was used for merging datasets where necessary, EMAN2 (Tang et al., 2007) was used for basic imaging processing tools, and Chimera (Goddard et al., 2007) was used for visualization purposes.

Light microscopy

Blood smears were stained with the WG16-500 ml kit for sickle cell assessment. Blood smears were observed using a 100× oil immersion objective on an Olympus BX60 microscope. Areas where RBCs did not overlap were randomly picked, and at least 10 fields were observed and 1000

RBCs, including sickle cells, were counted. Besides the obvious sickle-shaped cells, we considered the reversible sickle cells with sharp and pointed protrusions and deformed cells with aberrant morphologies as sickle cells. The percentage of sickle cells of the total RBCs was calculated (Zhang et al., 2011).

Measurement of lifespan of RBCs in SCD Tg mice

SCD Tg mice were treated with or without compound 5C for 28 days. At 21 days treatment, RBCs were labeled *in vivo* by using N-hydroxysuccinimide (NHS)-biotin and the lifespan of circulating RBCs was measured. Specifically, 50 mg/kg of body weight NHS-biotin was injected into the retro-orbital plexus of SCD mice. Blood samples (5 µl) were collected the first day after biotin injection, from the tail vein by venipuncture, to determine the percentage of RBCs labeled with biotin. Subsequently, 5 µl of blood was obtained by tail vein venipuncture every 3 days for measurement of biotinylated RBCs until the eighth day. The percentage of biotinylated RBCs was calculated by determining the fraction of peripheral blood cells labeled with a streptavidin-conjugated fluorochrome by flow cytometry (Zhang et al., 2011).

Statistical analysis

Data were analyzed for statistical significance using SAS software Version 9.2 (SAS Institute Inc., Cary, NC). The protrusion number data, presented in Figs 3 and 4, was first analyzed without binning and showed statistical significance between groups (data not shown). However, due to the noisy nature of this data, binning into categories was necessary for display. Multiple arbitrary binning strategies were explored, including changing the total number of bins, and shifting the data included in each bin. In all cases, the statistical significance between groups was maintained. Therefore, the presented categorization of protrusion numbers is arbitrary, but robust, and represents a statistically significant phenomenon. Outliers were calculated by first binning the data as described in Fig. 2, followed by identifying the median, and the value corresponding to the 25th and 75th percentile (i.e. Q1 and Q3 boundary) of each bin. The IQR was calculated and outliers were identified as outside the bounds of one IQR amount from either the Q1 or Q3 boundary. Data identified as outliers was not removed from the dataset. One-way analysis of variance and Tukey's multiple comparison test were used to identify differences between the means of multiple groups. Pairwise χ^2 tests were used to further localize the differences between populations. $P<0.05$ was considered significant. Group comparison data is normalized to 100% and presented with the s.e.m.

Acknowledgements

The authors would like to thank Matthew Guzman and Jemba Jakana for their gracious help in reconstructing tomograms.

Competing interests

The authors declare no competing or financial interests.

Author contributions

M.C.D., Y.X., C.A.L. and W.C. designed the study. Y.Z. prepared the samples and performed the light microscopy and survival experiments. B.P.C., E.A.S., R.B. and M.C.D. froze and imaged the samples using SXT. M.C.D. processed the SXT image data, staged the cells, performed the volumetric analysis and wrote the manuscript. M.C.D. and M.F.S. analyzed the data. R.H.R. and M.C.D. performed statistical tests. All authors reviewed the manuscript before submission.

Funding

This research has been supported, in whole or in part, by National Institutes of Health [grant number PN2EY016525 to W.C., P41GM103832 to W.C. and P41GM103445 to C.A.L.]; and by the U.S. Department of Energy, Office of Biological and Environmental Research [grant number DE-AC02-05CH11231 to C.A.L.]; and through a National Institute of Biomedical Imaging and Bioengineering training grant [grant number T32EB009270 to M.C.D.] awarded to the Keck Center of the Gulf Coast Consortia. Deposited in PMC for release after 12 months.

Supplementary information

Supplementary information available online at
http://jcs.biologists.org/lookup/doi/10.1242/jcs.189225.supplemental

References

Abdulmalik, O., Safo, M. K., Chen, Q., Yang, J., Brugnara, C., Ohene-Frempong, K., Abraham, D. J. and Asakura, T. (2005). 5-hydroxymethyl-2-furfural modifies intracellular sickle haemoglobin and inhibits sickling of red blood cells. *Br. J. Haematol.* **128**, 552-561.

Akinsheye, I., Alsultan, A., Solovieff, N., Ngo, D., Baldwin, C. T., Sebastiani, P., Chui, D. H. K. and Steinberg, M. H. (2011). Fetal hemoglobin in sickle cell anemia. *Blood* **118**, 19-27.

Alvarez, S. E., Harikumar, K. B., Hait, N. C., Allegood, J., Strub, G. M., Kim, E. Y., Maceyka, M., Jiang, H., Luo, C., Kordula, T. et al. (2010). Sphingosine-1-phosphate is a missing cofactor for the E3 ubiquitin ligase TRAF2. *Nature* **465**, 1084-1088.

Brittenham, G. M., Schechter, A. N. and Noguchi, C. T. (1985). Hemoglobin S polymerization: primary determinant of the hemolytic and clinical severity of the sickling syndromes. *Blood* **65**, 183-189.

Brugnara, C. (2003). Sickle cell disease: from membrane pathophysiology to novel therapies for prevention of erythrocyte dehydration. *J. Pediatr. Hematol. Oncol.* **25**, 927-933.

Carragher, B., Bluemke, D. A., Gabriel, B., Potel, M. J. and Josephs, R. (1988). Structural analysis of polymers of sickle cell hemoglobin: I. Sickle hemoglobin fibers. *J. Mol. Biol.* **199**, 315-331.

Carzaniga, R., Domart, M.-C., Collinson, L. M. and Duke, E. (2014). Cryo-soft X-ray tomography: a journey into the world of the native-state cell. *Protoplasma* **251**, 449-458.

Chang, H., Ewert, S. M., Bookchin, R. M. and Nagel, R. L. (1983a). Comparative evaluation of fifteen anti-sickling agents. *Blood* **61**, 693-704.

Chang, H., Ewert, S. M. and Nagel, R. L. (1983b). Identification of 2-imidazolines as anti-sickling agents. *Mol. Pharmacol.* **23**, 731-734.

Charache, S. and Conley, C. L. (1964). Rate of Sickling of Red Cells during Deoxygenation of Blood from Persons with Various Sickling Disorders. *Blood* **24**, 25-48.

Chichón, F. J., Rodríguez, M. J., Pereiro, E., Chiappi, M., Perdiguero, B., Guttmann, P., Werner, S., Rehbein, S., Schneider, G., Esteban, M. et al. (2012). Cryo X-ray nano-tomography of vaccinia virus infected cells. *J. Struct. Biol.* **177**, 202-211.

Christoph, G. W., Hofrichter, J. and Eaton, W. A. (2005). Understanding the shape of sickled red cells. *Biophys. J.* **88**, 1371-1376.

Coletta, M., Alayash, A. I., Wilson, M. T., Benedetti, P. A., Evangelista, V. and Brunori, M. (1988). Single cell microspectroscopy reveals that erythrocytes containing hemoglobin S retain a 'memory' of previous sickling cycles. *FEBS Lett.* **236**, 127-131.

Datta, A., Loo, S. Y., Huang, B., Wong, L., Tan, S. S. L., Tan, T. Z., Lee, S.-C., Thiery, J. P., Lim, Y. C., Yong, W. P. et al. (2014). SPHK1 regulates proliferation and survival responses in triple-negative breast cancer. *Oncotarget* **5**, 5920-5933.

Dykes, G., Crepeau, R. H. and Edelstein, S. J. (1978). Three-dimensional reconstruction of the fibres of sickle cell haemoglobin. *Nature* **272**, 506-510.

Dykes, G. W., Crepeau, R. H. and Edelstein, S. J. (1979). Three-dimensional reconstruction of the 14-filament fibers of hemoglobin S. *J. Mol. Biol.* **130**, 451-472.

English, D., Brindley, D. N., Spiegel, S. and Garcia, J. G. N. (2002). Lipid mediators of angiogenesis and the signalling pathways they initiate. *Biochim. Biophys. Acta* **1582**, 228-239.

Fabry, M. E., Mears, J. G., Patel, P., Schaefer-Rego, K., Carmichael, L. D., Martinez, G. and Nagel, R. L. (1984). Dense cells in sickle cell anemia: the effects of gene interaction. *Blood* **64**, 1042-1046.

Frenette, P. S. and Atweh, G. F. (2007). Sickle cell disease: old discoveries, new concepts, and future promise. *J. Clin. Invest.* **117**, 850-858.

Fygenson, D. K., Marko, J. F. and Libchaber, A. (1997). Mechanics of Microtubule-Based Membrane Extension. *Phys. Rev. Lett.* **79**, 4497-4500.

Goddard, T. D., Huang, C. C. and Ferrin, T. E. (2007). Visualizing density maps with UCSF Chimera. *J. Struct. Biol.* **157**, 281-287.

Hänel, P., Andréani, P. and Gräler, M. H. (2007). Erythrocytes store and release sphingosine 1-phosphate in blood. *FASEB J.* **21**, 1202-1209.

Hanssen, E., Knoechel, C., Dearnley, M., Dixon, M. W. A., Le Gros, M., Larabell, C. and Tilley, L. (2012). Soft X-ray microscopy analysis of cell volume and hemoglobin content in erythrocytes infected with asexual and sexual stages of Plasmodium falciparum. *J. Struct. Biol.* **177**, 224-232.

Harrington, D. J., Adachi, K. and Royer, W. E. Jr (1997). The high resolution crystal structure of deoxyhemoglobin S. *J. Mol. Biol.* **272**, 398-407.

Hassell, K. L. (2010). Population estimates of sickle cell disease in the U.S. *Am. J. Prev. Med.* **38**, S512-S521.

Herrick, J. B. (1910). Peculiar elongated and sickle-shaped red blood corpuscles in a case of severe anemia. *JAMA* **312**, 1063.

Horiuchi, K., Ballas, S. K. and Asakura, T. (1988). The effect of deoxygenation rate on the formation of irreversibly sickled cells. *Blood* **71**, 46-51.

Ikuta, T., Thatte, H. S., Tang, J. X., Mukerji, I., Knee, K., Bridges, K. R., Wang, S., Montero-Huerta, P., Joshi, R. M. and Head, C. A. (2011). Nitric oxide reduces sickle hemoglobin polymerization: potential role of nitric oxide-induced charge alteration in depolymerization. *Arch. Biochem. Biophys.* **510**, 53-61.

Journal of Cell Science

Ingram, V. M. (1957). Gene mutations in human hæmoglobin: the chemical difference between normal and sickle cell hæmoglobin. *Nature* **180**, 326-328.
Ito, K., Anada, Y., Tani, M., Ikeda, M., Sano, T., Kihara, A. and Igarashi, Y. (2007). Lack of sphingosine 1-phosphate-degrading enzymes in erythrocytes. *Biochem. Biophys. Res. Commun.* **357**, 212-217.
Kaul, D. K. and Xue, H. (1991). Rate of deoxygenation and rheologic behavior of blood in sickle cell anemia. *Blood* **77**, 1353-1361.
Kremer, J. R., Mastronarde, D. N. and McIntosh, J. R. (1996). Computer visualization of three-dimensional image data using IMOD. *J. Struct. Biol.* **116**, 71-76.
Kumar, A. A., Patton, M. R., Hennek, J. W., Lee, S. Y. R., D'Alesio-Spina, G., Yang, X., Kanter, J., Shevkoplyas, S. S., Brugnara, C. and Whitesides, G. M. (2014). Density-based separation in multiphase systems provides a simple method to identify sickle cell disease. *Proc. Natl. Acad. Sci. USA* **111**, 14864-14869.
Larabell, C. A. and Nugent, K. A. (2010). Imaging cellular architecture with X-rays. *Curr. Opin. Struct. Biol.* **20**, 623-631.
Le Gros, M. A., McDermott, G. and Larabell, C. A. (2005). X-ray tomography of whole cells. *Curr. Opin. Struct. Biol.* **15**, 593-600.
Le Gros, M. A., McDermott, G., Cinquin, B. P., Smith, E. A., Do, M., Chao, W. L., Naulleau, P. P. and Larabell, C. A. (2014). Biological soft X-ray tomography on beamline 2.1 at the Advanced Light Source. *J. Synchrotron Radiat.* **21**, 1370-1377.
Myllys, M., Ruokolainen, V., Aho, V., Smith, E. A., Hakanen, S., Peri, P., Salvetti, A., Timonen, J., Hukkanen, V., Larabell, C. A. et al. (2016). Herpes simplex virus 1 induces egress channels through marginalized host chromatin. *Sci. Rep.* **6**, 28844.
Noguchi, C. T. and Schechter, A. N. (1981). The intracellular polymerization of sickle hemoglobin and its relevance to sickle cell disease. *Blood* **58**, 1057-1068.
Noguchi, C. T., Rodgers, G. P., Serjeant, G. and Schechter, A. N. (1988). Levels of fetal hemoglobin necessary for treatment of sickle cell disease. *N. Engl. J. Med.* **318**, 96-99.
Padlan, E. A. and Love, W. E. (1985). Refined crystal structure of deoxyhemoglobin S. II. Molecular interactions in the crystal. *J. Biol. Chem.* **260**, 8280-8291.
Pappu, R., Schwab, S. R., Cornelissen, I., Pereira, J. P., Regard, J. B., Xu, Y., Camerer, E., Zheng, Y.-W., Huang, Y., Cyster, J. G. et al. (2007). Promotion of Lymphocyte Egress into Blood and Lymph by Distinct Sources of Sphingosine-1-Phosphate. *Science* **316**, 295-298.
Parkinson, D. Y., McDermott, G., Etkin, L. D., Le Gros, M. A. and Larabell, C. A. (2008). Quantitative 3-D imaging of eukaryotic cells using soft X-ray tomography. *J. Struct. Biol.* **162**, 380-386.
Patwardhan, A., Ashton, A., Brandt, R., Butcher, S., Carzaniga, R., Chiu, W., Collinson, L., Doux, P., Duke, E., Ellisman, M. H. et al. (2014). A 3D cellular context for the macromolecular world. *Nat. Struct. Mol. Biol.* **21**, 841-845.
Pauling, L., Itano, H. A., Singer, S. J. and Wells, I. C. (1949). Sickle cell anemia, a molecular disease. *Science* **110**, 543-548.
Pérez-Berná, A. J., Rodríguez, M. J., Chichón, F. J., Friesland, M. F., Sorrentino, A., Carrascosa, J. L., Pereiro, E. and Gastaminza, P. (2016). Structural changes in cells imaged by soft x-ray cryo-tomography during hepatitis c virus infection. *ACS Nano* **10**, 6597-6611.
Perutz, M. F., Rossmann, M. G., Cullis, A. F., Muirhead, H., Will, G. and North, A. C. T. (1960). Structure of Hæmoglobin: A Three-Dimensional Fourier Synthesis at 5.5-|[angst]|. Resolution, Obtained by X-Ray Analysis. *Nature* **185**, 416-422.
Pierre, R. V. (2002). Red cell morphology and the peripheral blood film. *Clin. Lab. Med.* **22**, 25-61.
Presley, T. D., Perlegas, A. S., Bain, L. E., Ballas, S. K., Nichols, J. S., Sabio, H., Gladwin, M. T., Kato, G. J. and Kim-Shapiro, D. B. (2010). Effects of a Single Sickling Event on the Mechanical Fragility of Sickle Cell Trait Erythrocytes. *Hemoglobin* **34**, 24-36.
Pruggnaller, S., Mayr, M. and Frangakis, A. S. (2008). A visualization and segmentation toolbox for electron microscopy. *J. Struct. Biol.* **164**, 161-165.
Ratajczak, M. Z., Lee, H., Wysoczynski, M., Wan, W., Marlicz, W., Laughlin, M. J., Kucia, M., Janowska-Wieczorek, A. and Ratajczak, J. (2010). Novel insight into stem cell mobilization-Plasma sphingosine-1-phosphate is a major chemoattractant that directs the egress of hematopoietic stem progenitor cells from the bone marrow and its level in peripheral blood increases during mobilization due to activation of complement cascade/membrane attack complex. *Leukemia* **24**, 976-985.
Rees, D. C., Williams, T. N. and Gladwin, M. T. (2010). Sickle-cell disease. *Lancet* **376**, 2018-2031.
Rodgers, D. W., Crepeau, R. H. and Edelstein, S. J. (1987). Pairings and polarities of the 14 strands in sickle cell hemoglobin fibers. *Proc. Natl. Acad. Sci. USA* **84**, 6157.
Sorette, M. P., Lavenant, M. G. and Clark, M. R. (1987). Ektacytometric measurement of sickle cell deformability as a continuous function of oxygen tension [published erratum appears in Blood 1987 Apr;69(4):1272]. *Blood* **69**, 316-323.
Spiegel, S. and Milstien, S. (2003). Sphingosine-1-phosphate: an enigmatic signalling lipid. *Nat. Rev. Mol. Cell Biol.* **4**, 397-407.
Tan, S. S. L., Khin, L. W., Wong, L., Yan, B., Ong, C. W., Datta, A., Salto-Tellez, M., Lam, Y. and Yap, C. T. (2014). Sphingosine kinase 1 promotes malignant progression in colon cancer and independently predicts survival of patients with colon cancer by competing risk approach in South asian population. *Clin. Transl. Gastroenterol.* **5**, e51.
Tang, G., Peng, L., Baldwin, P. R., Mann, D. S., Jiang, W., Rees, I. and Ludtke, S. J. (2007). EMAN2: An extensible image processing suite for electron microscopy. *J. Struct. Biol.* **157**, 38-46.
van Beers, E. J., Samsel, L., Mendelsohn, L., Saiyed, R., Fertrin, K. Y., Brantner, C. A., Daniels, M. P., Nichols, J., McCoy, J. P. and Kato, G. J. (2014). Imaging flow cytometry for automated detection of hypoxia-induced erythrocyte shape change in sickle cell disease. *Am. J. Hematol.* **89**, 598-603.
Wong, L., Tan, S. S. L., Lam, Y. and Melendez, A. J. (2009). Synthesis and evaluation of sphingosine analogues as inhibitors of sphingosine kinases. *J. Med. Chem.* **52**, 3618-3626.
Zhang, Y., Dai, Y., Wen, J., Zhang, W., Grenz, A., Sun, H., Tao, L., Lu, G., Alexander, D. C., Milburn, M. V. et al. (2011). Detrimental effects of adenosine signaling in sickle cell disease. *Nat. Med.* **17**, 79-86.
Zhang, Y., Berka, V., Song, A., Sun, K., Wang, W., Zhang, W., Ning, C., Li, C., Zhang, Q., Bogdanov, M. et al. (2014). Elevated sphingosine-1-phosphate promotes sickling and sickle cell disease progression. *J. Clin. Invest.* **124**, 2750-2761.